Modelling and Analysis of a Field-Circuit Model for the Hybrid Magnetic Bearing

Eng. Jamal Mohammed Shehata[1],
Eng. Majed Alshammari[2]
[1]Bachelor degree in Automotive Mechanics, Public Authority for Applied education and Training

Abstract:- This paper's proposed (HMB) model is dedicated and simulated to offer the transient condition. This model involves two components. The first section included mechanics and electrical circuits described by ordinary differential equations (ODF). Regarding the second section, several parameters are acquired from the simulated model, including velocity-induced voltages, magnetic forces, and dynamic inductances, which are acquired from the analysis. Regarding the simulation environment, MATLAB/Simulink environment was employed to conduct the proposed simulation model beside to desired control system. Then, the comparison process between the suggested HMB prototype with time responses was assisted in validating the proposed model of the field circuit.

Keywords:- Hybrid Magnetic Bearing, Ordinary Differential Equations, MATLAB/Simulink Software, HMB Prototype, Field Circuit.

I. INTRODUCTION

Repulsion, attraction, or magnetic force that appears between particles electrically charged due to their motion within its field. Regarding the magnetic force, a magnetic bearing (MB) denotes a machine with electromechanical behaviour(Samanta & Hirani, 2022). However, magnetic forces are utilised for several functions, such as suspending the rotor without resorting to mechanical contact. Consequently, MB is fitted and operated within high-speed machines because of their contactless process(Lomonova, 2010). A hybrid magnetic bearing (HMB) with a six-pole radial uses less electricity at 86.65% compared to the conventional active magnetic bearing (AMB) with an eight-pole at load capacity for both magnetic bearings (Wajnert, 2019). Nevertheless, permanent magnets could work to raise a magnetic leakage flux and increase the saturation within the magnetic circuit. Therefore, HMB's convoluted construction demands several ways to design dynamic simulations(Zhu, et al., 2017)
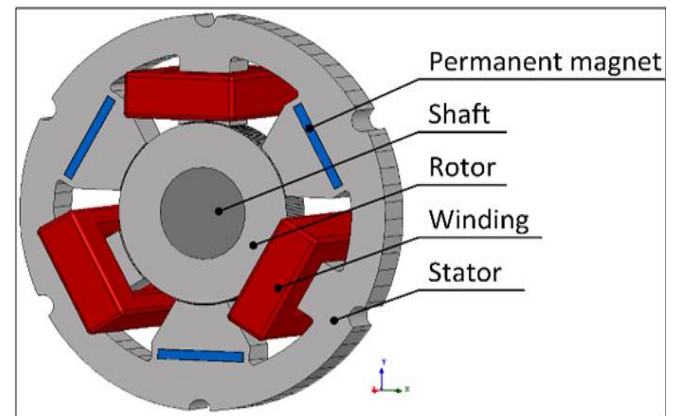.

Fig 1 Hybrid Magnetic Bearing

Based on AMB in this research (Singh & Tiwari, 2018), the study has been searched and investigated to regulate the identification possibility of the crack evidencing within the flexible rotor supported with the AMB approach. In addition, a splintered rotor with supported AMB inside the configuration of the auxiliary bearing has been studied and analysed to determine the supported end bearing stiffness and crack identification.

According to (Jabbar, et al., 2003), this research has suggested the time-stepping finite element (FEM) model to employ it with the AMB approach that includes two sections. The first section included mechanics and electrical circuits' ordinary differential equations (ODF). Regarding the second section, electromagnetic FEM that has two-dimensional (2D) with MB is analysed and solved by simulation. The suggested simulation model has several characteristics; for instance, it permits looking at hysteresis losses that occurred in the simulation model and eddy currents and has good accuracy. Nevertheless, the proposed model has one disadvantage involving the conventional solution of 2D to solve the magnetic field, and this phenomenon gives rise to critical errors in HMB. Meanwhile, 3D FEM rather than 2D contributes to increasing the time of the simulation.

According to (Wajnert, 2019), the Field- Circuit Method (FCM), Modified-Time-Stepping-Finite-Element-Method (MTSF), as well as the traditional Time-Stepping-Finite-Element (TSFE) Method have been utilised to calculate the transient current inside transformers. In this research, the authors have conducted a comparison between two methods, TSF and MTST, regarding their execution times for every approach. Therefore, while conducting the

comparison, it is noticed MTSF method is faster by two times than the traditional TSF method. Meanwhile, a one-phase transformer at two structures has been investigated and studied. In addition, at the end of this research, a comparison between the measured and calculated influx currents was made.

Referring to (Zhou, et al., 2020), in the presence of moveable variable mode and the complex distribution of spatial magnetic field, this study has implemented a torque analysis by employing the FEM method for spherical motors with time consumption and calculation. This study contributes to enhancing analysis efficiency by conducting a spherical motor and calculating torque analysis based on Lorentz force and the current model of the permanent-magnet surface. This approach aims to substitute the calculation of finite elements.

A system known as the MB system, which is composed of a PMB (permanent magnet bias) and a 2-axis active HMRB (high moment-to-rotor ratio bias), is presented in several studies. The PMB provides stiffness to hold the rotor in place when it is subject to gyroscopic forces, and also it gives a pivotal restoring force for the purpose of preserving the stability of the rotor throughout the length of the pivotal direction.Moreover, the HMRB gives a pivotal restoring force for the purpose of preserving the stability of the rotorin a plane at right angles to the rotor axis of rotation. Mathematical models for the PMB and HMRB are clarified in this paper. Several studies have analysed the bearing performance depending on the behaviour of torque angle and force position, in addition to the force current, utilising various techniques similar to the finite element analysis method (FEM), the equivalent magnetic circuit technique, as well as the magnetic charge equivalent technique(Han & Zheng, 2013).

The layout of the MBFW (Magnetic bearing flywheel) in an MSCMG (motor-generator-controller-magnet) system is depicted in Figure 1. The flywheel rotor is held in place by the PMB (permanent magnet bias) and the HMRB (high moment-to-rotor ratio bias). The PMB consists of two groups of rings composed of a permanent magnet. The different components of the MBFW at the subassembly level include the components clarified in Figure 1, where the PMB and the HMRB support the structure (Han & Zheng, 2013)
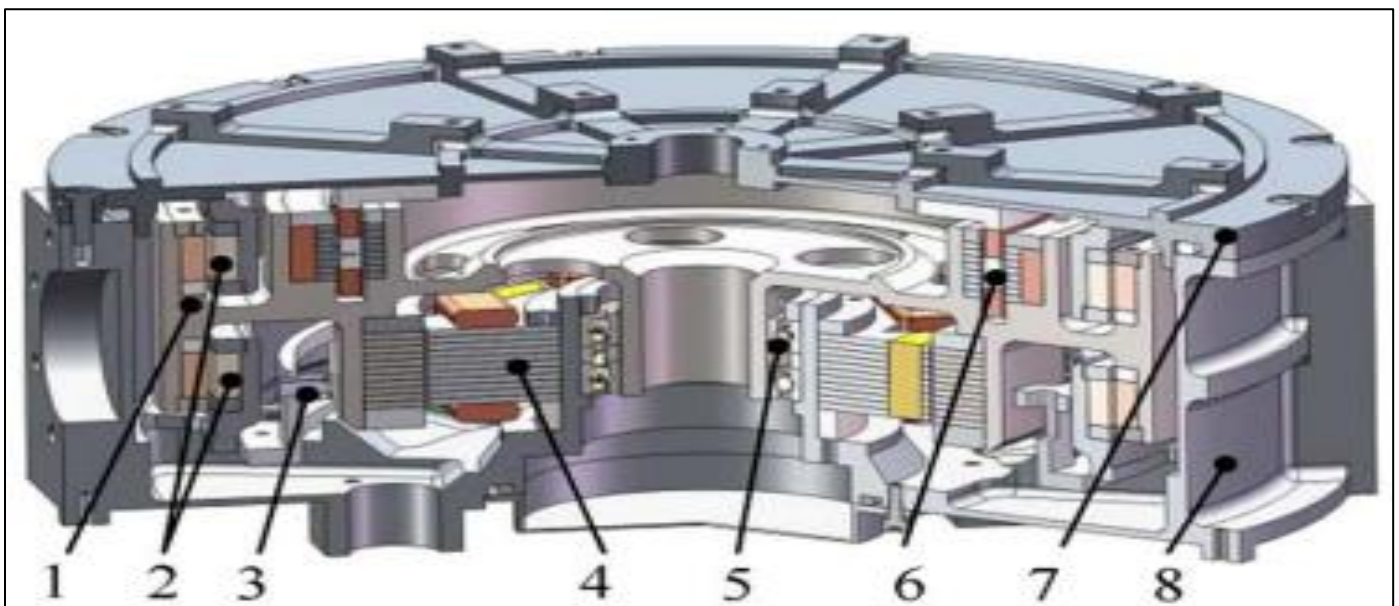

Fig 2 Configuration of Field-Circuit Model for the HMB Where 1- Denotes the Rotor while 2-Denotes the PMB and 3-Denotes the Displacement Sensor while 4-Denotes the Hybrid Magnetic Radial Bearing, Similarly 5-Denotes the Touch-Down Bearing, 6-Denotes the Drive Motor. Finally, 7-Denotes the Cover.

Most energetic magnetic bearing system (MBSs) typically consists of one unit of axial magnetic bearing (AMB) and two units of radial magnetic bearing (RMB). These MB designs are relatively easy to build, but they tend to be overweight, have high power, and are expensive. It is essential to lessen the number of modules by further integrating RMB and AMB to lessen the size, price, and power consumption and increase the MBS energy density.The combined radial-axial magnetic bearing (CRAMB), known as the 3-axis MB, is created for usage in machines operating at ultra-high-speed as a way to overcome these issues.

A study is conducted on analysing magnetic forces and coupling problems of a combined AMB and RMB. An incorporatedRMB and AMB using a conical shape rotor are createdand evaluated.Nevertheless, the combined bearings cause a strong coupling problem between axial and radial degrees of freedom. A proposed solution is the AC-DC of 3-DOF HMB, which is created. Its construction and control technique is defined in the literature. The 3-DOF axial HMB is also suggested, but it is complex in its structure and processing technique, and at a high-speed level, it has a considerable rotational power loss. An alternative is introduced with a 3-DOF MBlacking a massivedrive rotor

disk, and its design is presented. The literature offers a combined radial-axial MB, not including the axial disc, and its stationary implementation is examined by employing 3D FEM analysis. The stationary mathematical prototype of the radial-axial MB is also covered in the literature (Han, 2014).

This paper offers a 6-pole radial HMB in terms of the FCM method, which has several parameters such as velocity-induced voltages, dynamic inductances, and magnetic force. These parameters were derived by employing the analysis of 3D finite-element. The formulation of Euler-Lagrange has derived ordinary differential equations, where these equations contributed to defining the HMB circuit section. The MATLAB/Simulink software was employed to acquire the simulation model in the presence of desired controllers. This research aims to construct an HMB dynamic model to monitor strategy testing and analyse HMB's performance analysis.

II. RELATED WORKS

According to (Jin, et al., 2022), it has been pointed out that if the MB rotor is running, an iron loss phenomenon possibly will arise in the rotor, which will cause a thermal imbalance and temperature gradient. In order to investigate this phenomenon, a multiphysics (dual physical occurrences in processor simulations) simulation technique is suggested regarding thermomagnetic coupling. This technique is used employing conducting FEM in ANSYS Maxwell modelling to recognise the sources of the iron loss in the MB and the effect of several influences on the iron losses distribution and magnitude; COMSOL use of thermomagnetic coupling in an MB to realise the effect of iron loss on the phenomena of temperature distribution. The Ansys simulation findings specify that because of the early disturbance, the effect of MB control of triggering the distribution of the magnetic field to be uneven on the circumference of the MB rotor, causing the iron loss phenomenon. The bias current and control current greatly influence the distribution of iron loss, whereas the speed and bias current greatly influence the value of the iron loss. Therefore, the concentration of iron loss will cause a temperature gradient at the surface of the MB rotor. The FEM of thermomagnetic coupling is confirmed employing a temperature growth detection experiment. Also, it offers a reference and theoretical basis for MB's thermal loss and unbalances.

Similarly, another study conducted by (Szelag, et al., 2023)offered a field model of an integrated influence that takes place in a pivot magnetic brake. The presented model considers the coupling between the mechanical equilibrium formulas, fleeting fluid dynamics, and thermal fields. The magnetic field within the considered brakes is induced through a hybrid means, by both current flowing and permanent magnets through the excitation coil. The FEM technique and a phased algorithm were employed in the offered field model of integrated influence that takes place in a considered magnetic brake. The model considers the magnetic topology nonlinearity, the rheological characteristics of the magnetorheological fluid, and the impact of temperature gradient on the characteristics of the material. The coupled block over-relaxation and Newton–Raphson approaches were used to solve and analyse the obtained expressions of the magnetic field model. The established algorithm has been efficaciously employed to examine the occurrences in the regarded magnetorheological brake. Moreover, the established model's applicability and accuracy were confirmed by matching the simulation findings and the conducted laboratory tests on the brake prototype.

However, based on (Shi & Dong, 2022), it was stated that the impact of the vibration that produces harmonics must be studied and investigated, especially for permanent-magnet-synchronous-motor (PMSM). Approach analyses based on domain-circle coupling were presented. Furthermore, the examination process initiates from a control approach to a noise response and vibration of the engine in the motor. First, a coupling model comprising a control approach, an essential circuit model, and the electromagnetic field model, was constructed. Then, a FEM analysis of the PMSM model beneath the coupling effect was created to examine and associate sinusoidal and coupling excitations' electromagnetic force tendency properties. Afterwards, the coupled force was burdened on the structural domain to mimic and compute noise and vibration. Finally, the model's effectiveness was tested by comparing the experimental pressure level of sound beneath acceleration and steady-state conditions, which affords a reference for the motor model's prediction of noise and vibration. The field circuit structure is revealed in Figure 3.
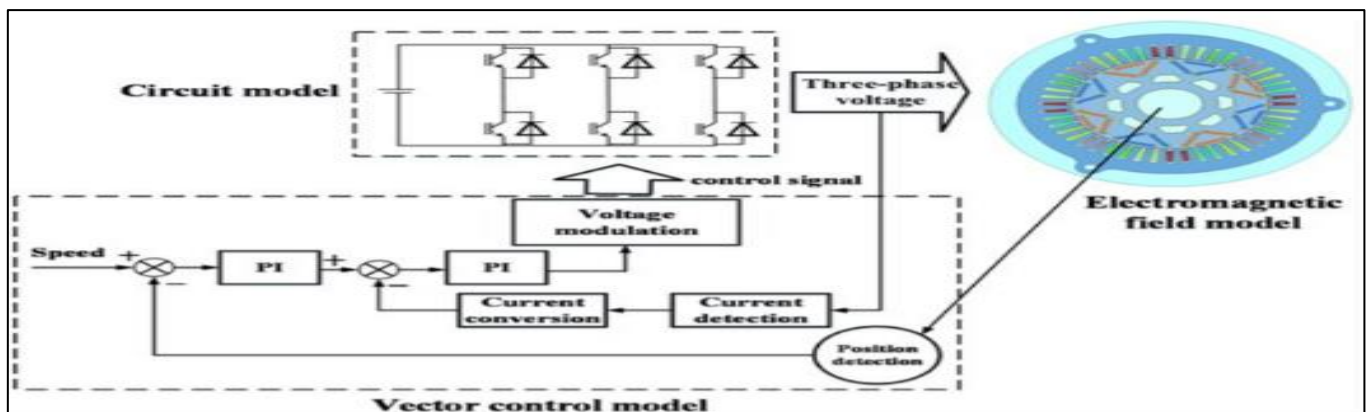

Fig 3 Coupling Structure of Field-Circuit

A study (Noshadi, 2019) examined a specific type of control system, known as Active Magnetic Bearings (AMBs), in reliable and high-speed usage. AMBs are attractive alternatives to hydrostatic bearings because they have no mechanical friction, very accurate, and have low maintenance costs. Nevertheless, they are characteristically unstable and necessitate closed feedback controllers for maintaining steadiness. The paper specifically looks at using an H loop-shaping techniquetomake the behaviour steadyin the adjustable shaft during the stationary condition and then introducing an inner loop to minimise vibration and improve performance at various rotational speeds. The techniqueintegratesproperties of common repetitive and disturbance observer-based types of controllers.
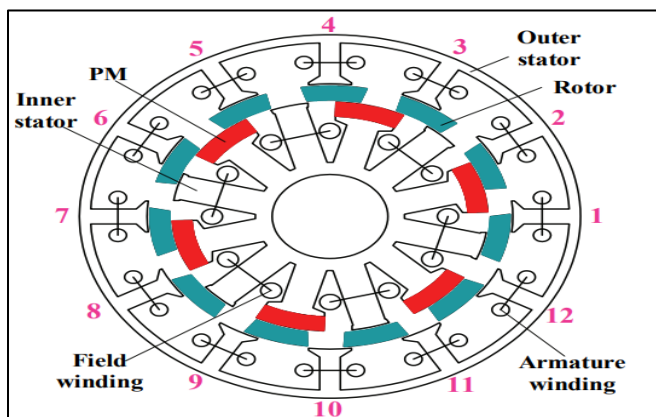

Fig 4 Configuration of the Field-Circuit Model Inside the Magnetic Bearing.

The suggested algorithm's usefulness, shown in Figure 4 is tested on a MIMO AMB (multi-input-multi-output) scheme, and the findings show that it can robustly stabilise the model and significantly reduce the harmonic disturbancesinfluence. Moreover, the HE machines, also known as hybrid excited machines, combine wound-field (WF) and Permanent Magnet (PM) machines. They offer a high level of both torque density and efficiency and good field controllability. These machines usefield windings (FWs) and PMssimultaneously, providing further freedom regarding the ratio of FW and PM fluxes. In the low-speed operating range, DC current in the positive cycle of operationwould be fed to the FWs for the purpose of increasing torque output. In contrast, DC current in the negative cycle of operationwould be fed to the FWs for the purpose of preserving a high power factor and extending the CPSR. The outcomes showed that by constructing a hybrid magnetic bearing, the modelling and analysis of a field circuit become more complicated, but the outcomes would be more reliable and satisfactions

III. THE HYBRID MAGNETIC BEARING (HMB)

The utilized HMB has six distinct poles, three of which have permanent magnets labelled N38, and the other has three windings. The permanent magnets are placed within the pole gaps to create a bias flux. Furthermore, the HMB's rotor and stator are made from a specific type of steel called M400-50A for decreasing the amount of eddy currents. This is because the steel M400-50A has a high magnetic

saturation point, allowing it to carry a higher magnetic field before reaching saturation, effectively reducing the eddy current losses.

A modification for the air gap (δ) magnitude stated as 0.30 mm will be done as the used (δ) value will be 0.39 mm to achieve a good result from the simulation model comparable to the actual object. A slight difference between the actual and simulated model is predicted due to the nonmagnetic layer created during the manufacturing with a length of (0.04, 0.05, and 0.07) mm(Wajnert & Tomczuk, 2019).

The magnetic poles expose the magnetic force effect because of an occurring flux between the stator and rotor. However, only the three poles with windings can regulate the magnetic force in three different directions, designated as s1, s2, and s3. The HMB rotor's location is managed through two controllers, one for the x-axis and one for the y-axis, by altering the (ix and iy) control currents. Furthermore, the currents in the windings i1, i2, and i3 can be obtained using the following equations:

$$\begin{bmatrix} i1 = iy \\ i2 = -\frac{1}{2}iy + \frac{\sqrt{3}}{2}ix \\ i3 = -\frac{1}{2}iy + \frac{\sqrt{3}}{2}ix \end{bmatrix} \quad (1)$$

Furthermore, the rotor position s1, s2, and s3 can be obtained using the following equations:

$$\begin{bmatrix} s1 = y \\ s2 = -\frac{1}{2}y + \frac{\sqrt{3}}{2}x \\ s3 = -\frac{1}{2}y + \frac{\sqrt{3}}{2}ix \end{bmatrix} \quad (2)$$

IV. MODEL OF FIELD CIRCUIT FOR HMB

Two components comprise the field circuit model, where the first part involves several differential equations. The differential equations are extracted from the Euler-Lagrange formulation. The HMB electrical circuit may be governed by the following:

$$u_1 = R_1 i_1 + L_{d1}(s_1, i_1) * \frac{di_1}{dt} + e_{v1}(s_1, i_1)\frac{ds_1}{dt} \quad (3)$$

$$u_2 = R_2 i_2 + L_{d2}(s_2, i_2) * \frac{di_2}{dt} + e_{v2}(s_2, i_2)\frac{ds_2}{dt} \quad (4)$$

$$u_3 = R_3 i_3 + L_{d3}(s_3, i_3) * \frac{di_3}{dt} + e_{v3}(s_3, i_3)\frac{ds_3}{dt} \quad (5)$$

In which u_1, u_2, and u_3 represent the supplying voltages while R_1, R_2, and R_3, denote the windings resistances, and L_{d1}, L_{d2}, and L_{d3}, represent the windings dynamic inductances. Finally, e_{v1}, e_{v2}, and e_{v3} denote the velocity-induced voltages. As mentioned before, the HMB mechanics may be controlled effectively by the following mathematical equations:

$$m\frac{d^2x}{dt^2} = F_x(x, i_x) + m\omega^2 e_s \cos(\omega t) \qquad (6)$$

$$m\frac{d^2y}{dt^2} = F_y(x, i_y) - mg + m\omega^2 e_s \sin(\omega t)$$

The symbols F_x & F_y represent the magnetic forces applied in both the x-axis and y-axis. While e_s represents the eccentricity, ω represents the rotational speed, and finally, the symbol m represents the rotor mass, and g refers to the gravity acceleration.

The second part involves several parameters, such as the dynamic inductance identified as L_{d1}, L_{d2}, and L_{d3}, the velocity-induced voltages e_{v1}, e_{v2}, and e_{v3} in addition to the magnetic forces F_x and F_y.

Half of the geometry of the real object is constituted within the FEM to minimize the tetrahedral number of elements. In the simulation, the calculation domains were divided into smaller sections using an adaptive meshing technique. The boundaries of the studied simulation model have been positioned 40 mm away from the rotor and stator, except for the level of symmetry, which was positionedat mid the length of the stator.In contrast, the simulation model's outer surface was given a zero Dirichlet boundary condition, while a symmetry plane was given a zero value of the Neumann boundary condition. The magnetic material's nonlinear behaviour was evaluated using a closed magnetic circuit (Tomczuk & Koteras, 2015). The solution for the distribution of the magnetic field was obtained using a magneto static solver that employs the T~-Ω approach. Moreover, the (H~) magnetic field was signified by a combination of the magnetic scalar potential (known as Ω) and the current vector potential (known as T~) (Badics & Cendes, 2007).

$$\vec{H} = \vec{T} + \nabla\Omega \qquad (7)$$

Where the symbol $\vec{H}$ represents the magnetic field, $\vec{T}$ achieves the following equation:

$$\nabla \times \vec{T} = \vec{J} \qquad (8)$$

Where $\vec{J}$ represents the current density. Generally, the magnetic field in the current free spaces can be determined by the magnetic scalar potential Ω:

$$\vec{H} = \nabla\Omega$$

The applied magnetics forces F_x, F_y, and F_z, represented in Figure 5, may be calculated by the virtual work approach:

$$F_x(x, i_x) = \frac{\partial W_{co}(x, i_x)}{\partial x}\bigg|_{i_x} = constant \qquad (9)$$

$$F_y(x, i_y) = \frac{\partial W_{co}(y, i_y)}{\partial y}\bigg|_{i_y} = constant \qquad (10)$$

Where the symbol W_{co} represents the HMB of the energy. However, the ψ, magnetic flux linkage, has been found by applying the following formula:

$$\psi = N \iint_S \vec{B}.d\vec{S}, \qquad (11)$$

The term N represents the stator winding turn number and the term S represents the pole area. The linkages ψ_1, ψ_2, ψ_3 have been employed in order to determine the velocity-induced voltages and the dynamic inductances based on the following mathematical expressions:

$$L_{d1}(s_1, i_1) = \frac{\partial\psi_1(s_1, i_1)}{\partial i_1} \qquad (12)$$

$$L_{d2}(s_2, i_2) = \frac{\partial\psi_2(s_2, i_2)}{\partial i_2}$$

$$L_{d3}(s_3, i_3) = \frac{\partial\psi_2(s_3, i_3)}{\partial i_3}$$

$$e_{v1}(s_1 i_1) = \frac{\partial\psi_1(s_1, i_1)}{\partial s_1} \qquad (13)$$

$$e_{v2}(s_2 i_2) = \frac{\partial\psi_2(s_2, i_2)}{\partial s_2}$$

$$e_{v3}(s_3 i_3) = \frac{\partial\psi_3(s_3, i_3)}{\partial s_3}$$

Because of the symmetry in HMB, the velocity-induced voltages e_{v2}, e_{v3}, and the dynamic inductances L_{d2} and L_{d3} were identical to the dynamic inductance L_{d1} and the e_{v1}.

The displacement stiffness and the current are critical in designing the magnetic bearing's control. Table 1 shows the HBM parameters and the lack of control currents determined for the central rotor position

Table 1 HMB Parameters

Parameter	Velocity-induced voltage, e_v	Dynamic inductance, L_d	Current stiffness, k_{iy}	Position stiffness, k_{ry}	Current stiffness, k_{ix}	Position stiffness, k_{rx}
Value	13.86 Vs/m	4.67 mH	20.60 N/A	124.83 N/mm	20.50 N/A	20.50 N/A

V. THE FIELD-CIRCUIT MODEL USING MATLAB/SIMULINK SOFTWARE

The control scheme plays a crucial function in the MB system because it enables the rotor to be liftedand determines its entire performance. Various control systems have been studied, such as PD, LQR, and PID (Srinivas, et al., 2018). Among these, the PID (proportional-integral-derivative) controller represents the most frequently universally employed due to its ease. Furthermore, position PID controllers are frequently utilised in conjunction with the current control method (Kushwah & Patra, 2014). Figure 5 illustrates the FCM integration with a control scheme using MATLAB/Simulink environment.
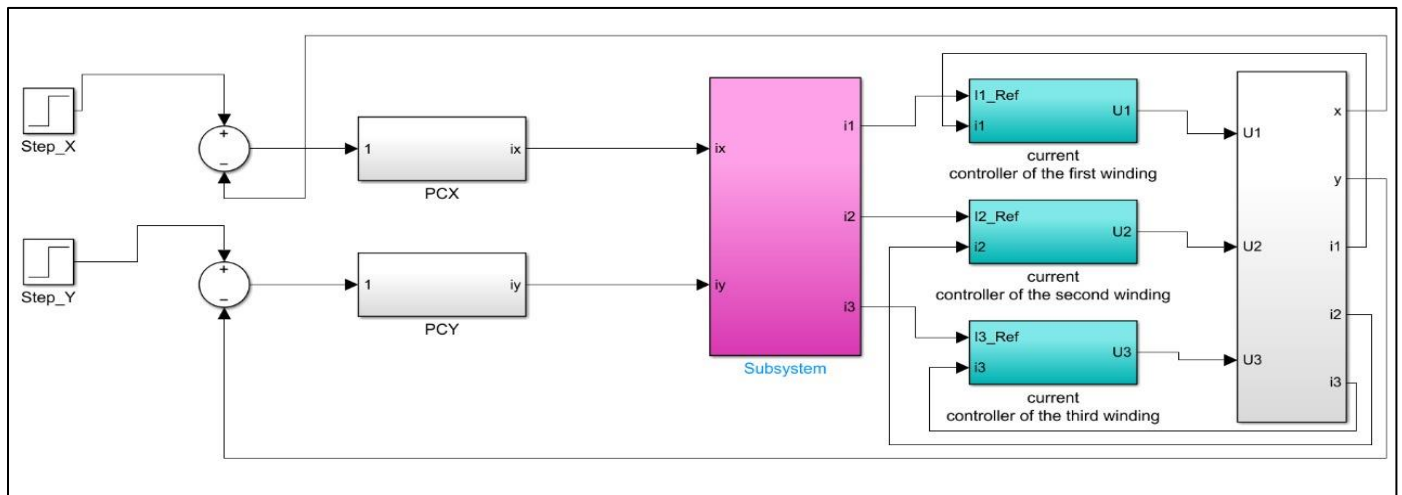
Fig 5 The Control Scheme Being Executed Using the MATLAB/Simulink Environment. The System Includes Controllers for the Position In the X and Y Axes (PCX And PCY) as well as Controllers for the Current In Three Different Windings (CC1, CC2, andCC3).

Both the internal feedback loop and external feedback loop are included in the control system. The internal feedback loop maintains the stability of the current in the HMB winding. Three current controllers are included in the internal loop (CC1, CC2, and CC3) with power amplifiers and HMB's power equations. However, the stability of the rotor position is maintained by the external feedback loop, which is made up of dual position controllers (PCX and PCY) with a conversion block that converts control currents into windings currents; the main loop used in the current control process, as well as the HMB's mechanical equations. Furthermore, the subsystem "HMB" represents the FCM implementation as outlined in Equation 1 through Equation 4 and is illustrated in Figure 6.
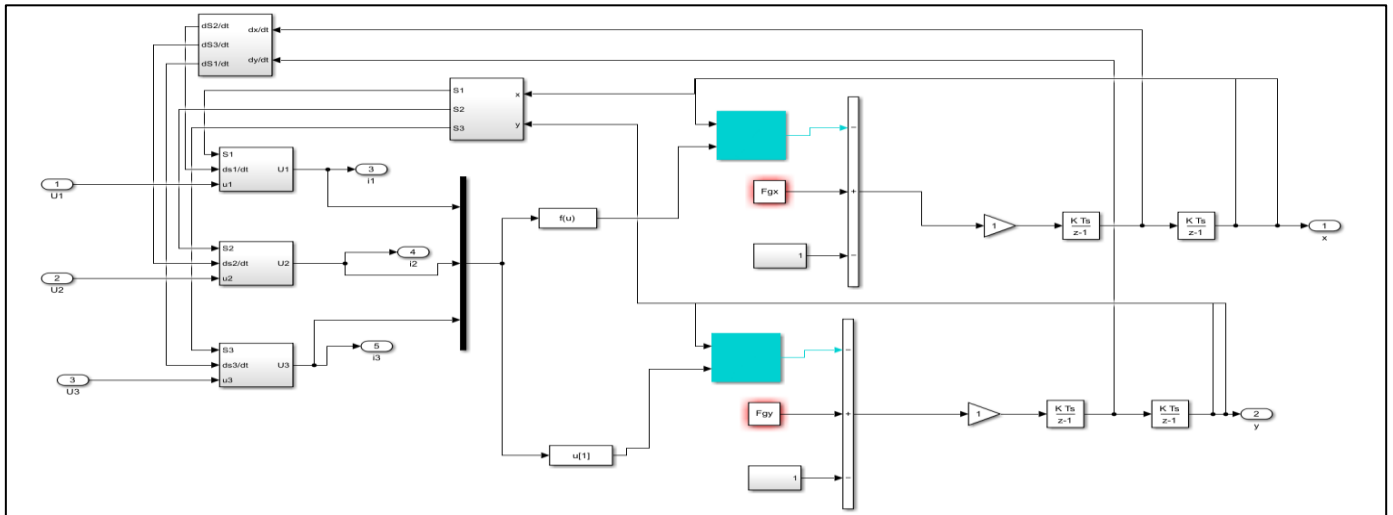
Fig 6 The HMB Simulation Model

In Figure 7, the system includes look-up tables labelled $F_x\,(x, i_x)$ and $F_y\,(y, i_y)$, which contain previously computed magnetic force traits in both the x and y axes. The three subsystems labelled (Winding No.1), (Winding No.2), and (Winding No.3) implement the HMB electrical Equations(3). Thus, in Figure 9, equation (3a) is implemented to describe and define the first winding. The look-up tables labelled $L_{d1}\,(s_1, i_1)$ and $e_{v1}(s_1, i_1)$ include computed traits of the dynamic inductance and the voltage induced by velocity.
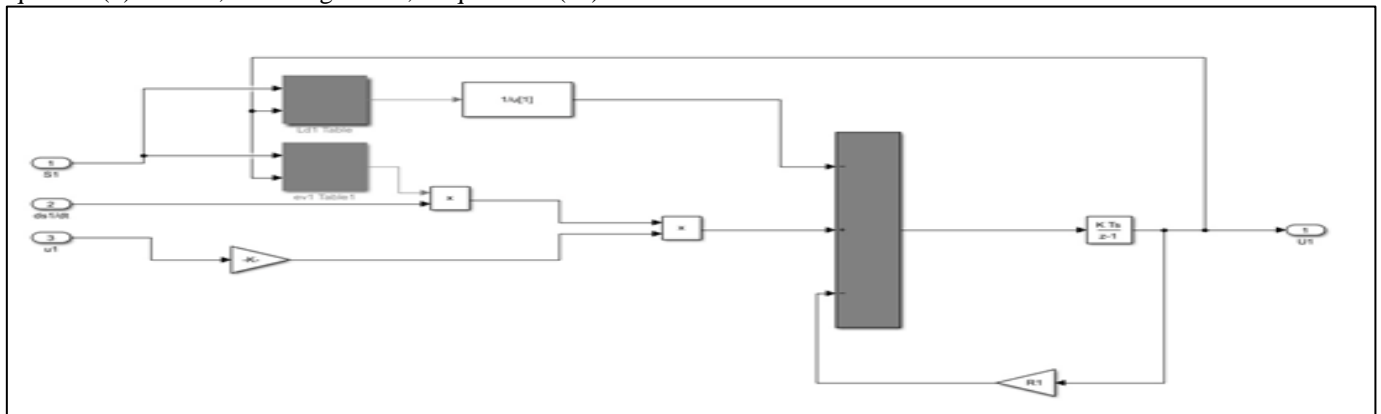
Fig 7 The First Winding Simulation Model.

The HMB linear model is used to obtain the control system's parameters. A set of equations below describes the

$$m\,\frac{d^2x}{dt^2} = k_{sx}x + k_{ix}i_x \qquad (13\ a)$$

$$m\,\frac{d^2y}{dt^2} = k_{sy}y + k_{iy}i_y \qquad (13b)$$

The point of linearisation for the HMB's magnetic force is obtained from the permanent magnets and magnetic circuit systems. Furthermore, for the specific HMB being discussed, the bias flux equals 76.1 mWb. Also, the density of the magnetic field is 0.634 T, which is for the magnetic field in poles in conjunction with the permanent magnets. Two separated PID controllers manage the rotor's position in the two axes. Noting that K_P, K_1, and K_D are variables used in a controller, and T_s represents the interval at which data is collected. N Represents the value used to filter data in the derivative calculation.

$$G_{PID}(z) = (K_P) + (K_1\,\frac{T_s}{z-1}) + (K_D\,\frac{N}{1+\frac{T_sN}{z-1}}) \qquad (14)$$

The currents in the windings, denoted by (i_1, i_2, and i_3), are regulated by 3 PI controllers that operate at discrete intervals.

$$G_{PI}(z) = (K_P) + (K_1\,\frac{T_s}{z-1}) \qquad (15)$$

All controllers have an anti-windup circuit to prevent integrator windup (Premkumar, et al., 2019). Such controllers have parameters that can be determined using analytical formulas as follows:

$$K_p = [(p_1p_2 + p_2p_3 + p_1p_3)m - k_s]/k_i \qquad (16\ a)$$

$$K_I = [(-p_1p_2p_3)m]/k_i \qquad (16\ b)$$

$$K_D = [(-p_1 - p_2 - p_3)m]/k_i \qquad (16\,c)$$

The variables p_1, p_2, and p_3 represent the necessary poles for the control system to function correctly. Thus, these poles determined the MB system's dynamic response and are defined as follows. Noting that ω_n is the natural frequency of the system without any damping, and ξ represents the damping ratio, both of which are used to define the complex poles p_1 and p_2.

$$p_1, p_2 = -\omega_n\xi \mp j\omega_n\sqrt{1-\xi^2} \qquad (17)$$

The value of p_3 should not affect the MB system's dynamic response. The values of p_1 and p_2 can be found by comparing the characteristics of a 2nd order equation to those of a mass-spring-damper system, and different expressions can be used to calculate them and the damping coefficient c and the stiffness coefficient k are used in the expressions for computing the complex poles p_1, p_2, and p_3.

$$p_1, p_2 = -\frac{c}{2m} \mp j\sqrt{\frac{k}{m} - \frac{c^2}{4m^2}} \qquad (18)$$

$$p_3 = \sqrt{k/m} \qquad (19)$$

Both factors k and c are commonly used to compare different bearing types, in which the PID controllers' parameters were calculated using equation (17) and equation (18) with $30000\ N/m$ and $100\ Ns/m$ as stiffness value of k and a damping coefficient, respectively. The PI current controllers 'parameters were set through manual modification to achieve and ensure acceptable overshooting with a fast response. Table 2 shows the position controller coefficients values and the current controller coefficients values.

Table 2 The Position and Current Controller Coefficients.

The position controller coefficients (values)		
	x-axis	y-axis
$K_P \left(\frac{A}{m}\right)$	8,424	8,852
$K_I \left(\frac{As}{m}\right)$	120,342	126,500
$K_D \left(\frac{A}{ms}\right)$	13.03	15.26
The current controller coefficients (values)		
$K_P \left(\frac{A}{m}\right)$	0.35	
$K_I \left(\frac{As}{m}\right)$	400	

VI. RESULTS AND DISCUSSION

Figure 8 depicts the test bench's general layout of the

HMB's control system. Furthermore, the actuator is considered a computer with a controller board of DS-1104 R&D, current transducers, proximity sensors, semiconductor power amplifiers, and the verify the bench. Also, there are 3 LEM LTS-6NP sensors utilised for measuring current levels. In addition, 2- eddy current proximity sensors with MDS10/MDT10 monitor the gap between the rotor and stator. Their measuring range is between 0.5 mm and 2.5 mm, with a 10 kHz frequency response.
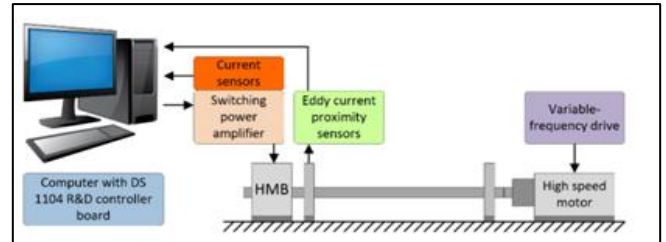

Fig 8 The Test Bench's General Layout of the HMB's Control System

The DS1104 board accomplishes several tasks converting position signals and current from analogue - to - digital; running 3-PI current controllers; running 2-PID position controllers; and producing PWM signals that switch power amplifiers. Furthermore, both (12-bit A/D) and 1 (16-bit A/D) converters are present on the (DS-1104 R&D) controller board.

The four-channel analogue multiplexer is also implemented on the (16-bit A/D) converter. The entire A/D converters employ an inner sample-and-hold circuit and a successive approximation technique for converting the analogue signal into a digital value. In addition, four (12-bit A/D) converters of a combined resolution of 1.693 mA/bit and a frequency of 20 kHz concurrently transform the current signal. Also, the (16-bit A/D) converter of frequency equals 10 kHz with a resolution of 0.03815 m/bit converts the position signals in both the x and y axes. The delay among two rotor position samples should not exceed two μs. Also, the semiconductorpower amplifiers operate at a frequency equal to 50 kHz.

Furthermore, the FCM was verified by comparing the time responses gained as a result of the simulation modelling of the actual objects. Three dynamic states were taken into account: a step change of ±20 μm for the x-axis, a step change of ±20 μm for the y-axis, as well as the rotation position of the rotor with a frequency equal to 100 Hz. Figure 9 illustrates the time response results of the control currents.
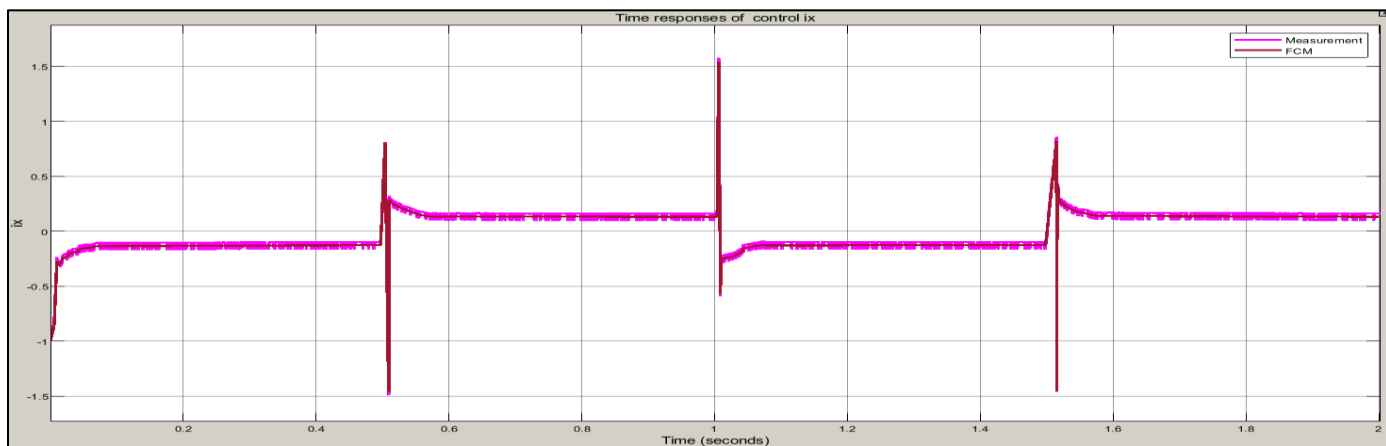
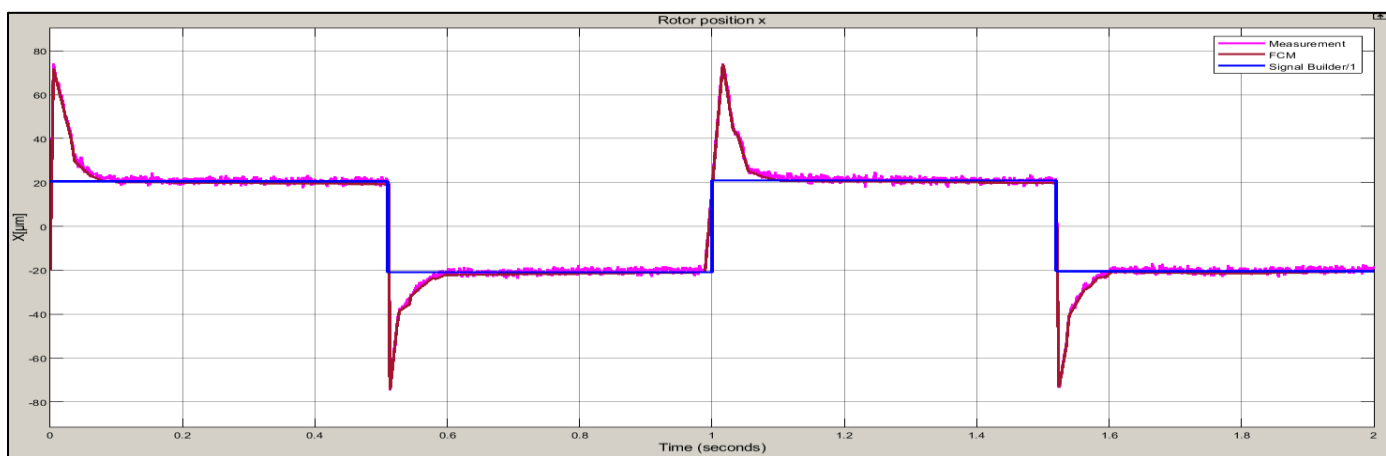Fig 9 The Time Responses Results of the Control Currents: (a) Rotor Position is (X)

Fig 9 The Time Responses Results of the Control Currents: (b) Control Current is (Iy)
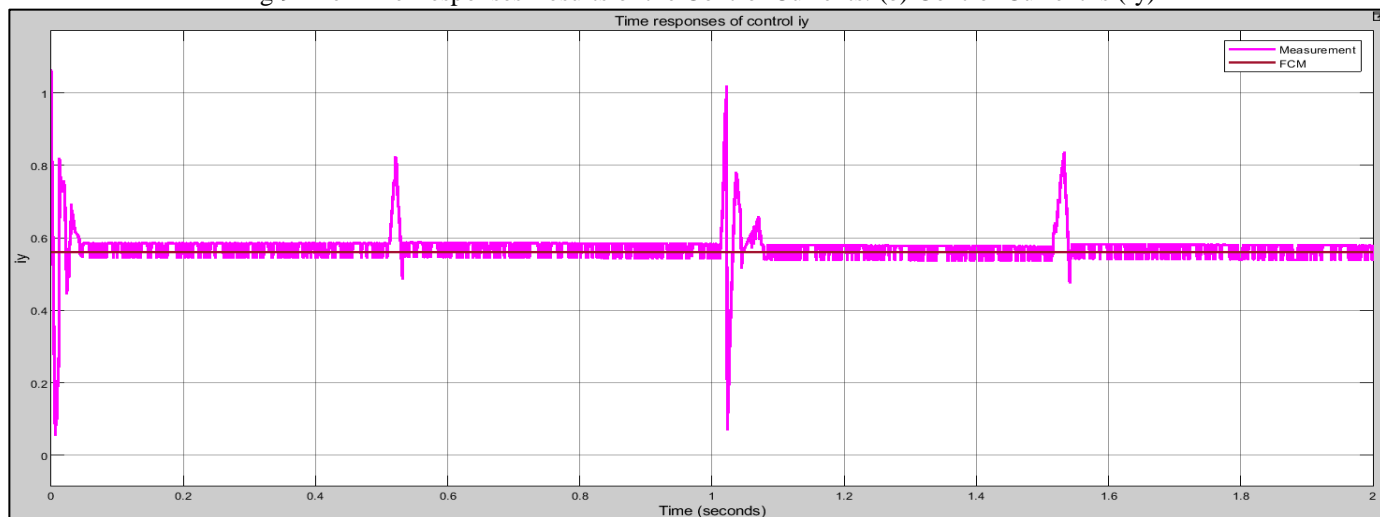

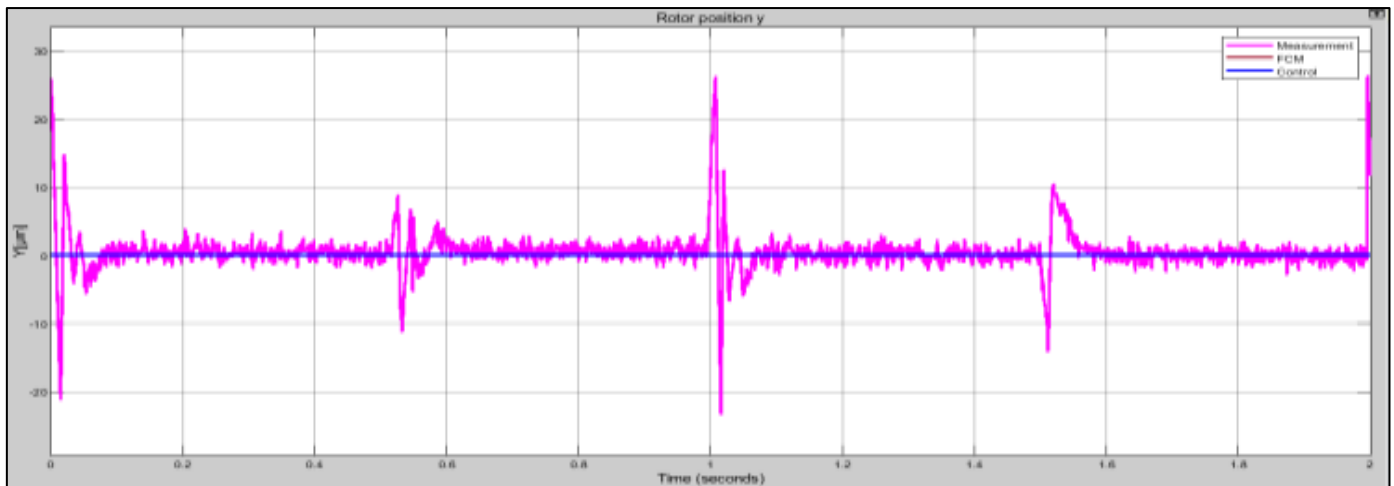Fig 9 The Time Responses Results of the Control Currents: (c) Rotor Position is (Y)

Fig 9 The Time Responses Results of the Control Currents: (d) Step Change is ±20μm of the Position of the Rotor.

An observable interference signal that appears in the measurements is the result of the amplifiers of the switching power, as well as the inadequate electromagnetic protection of the analogy signals.

However, in the actual object, there is a clear rotation position of the rotor disturbance in the orthogonal axis to the axis with the rotor position's step change, shown in Figure 8/b. This behaviour designates cross-coupling in the two axes, which leads to a noteworthy change in the orthogonal axis of the control current. The time response of the i_x control current, in addition to the rotation position of the rotor in the two axes with a step change equal to ±20 μm, is represented in Figure 10.
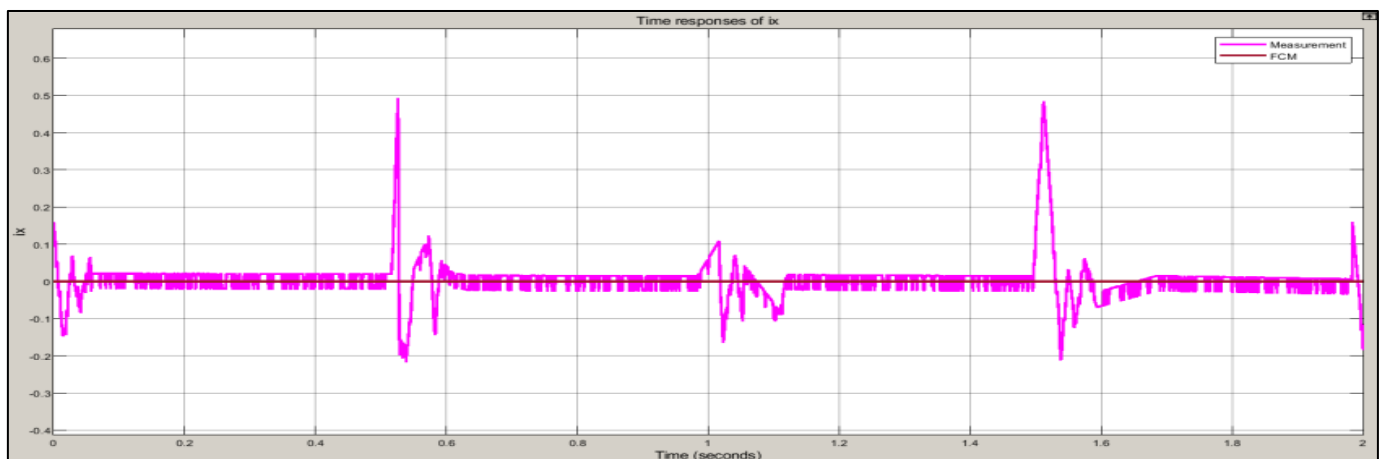

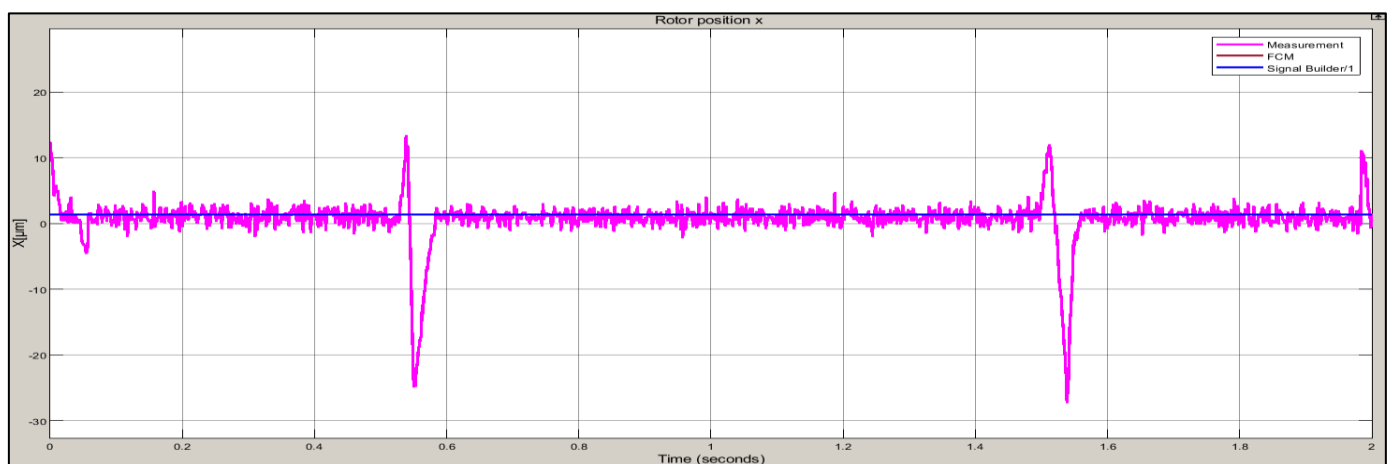Fig 10 The Time Responses Results of the Control Currents: (a) Rotor Position is (X)

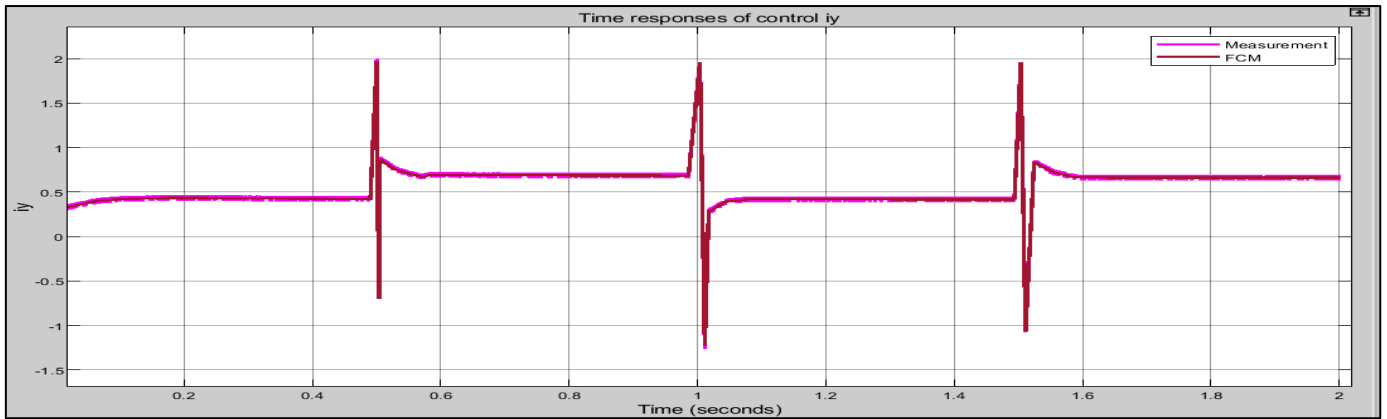Fig 10 The Time Responses Results of the Control Currents: (b) Control Current is (Iy)

Fig 10 The Time Responses Results of the Control Currents: (c) Rotor Position is (Y)
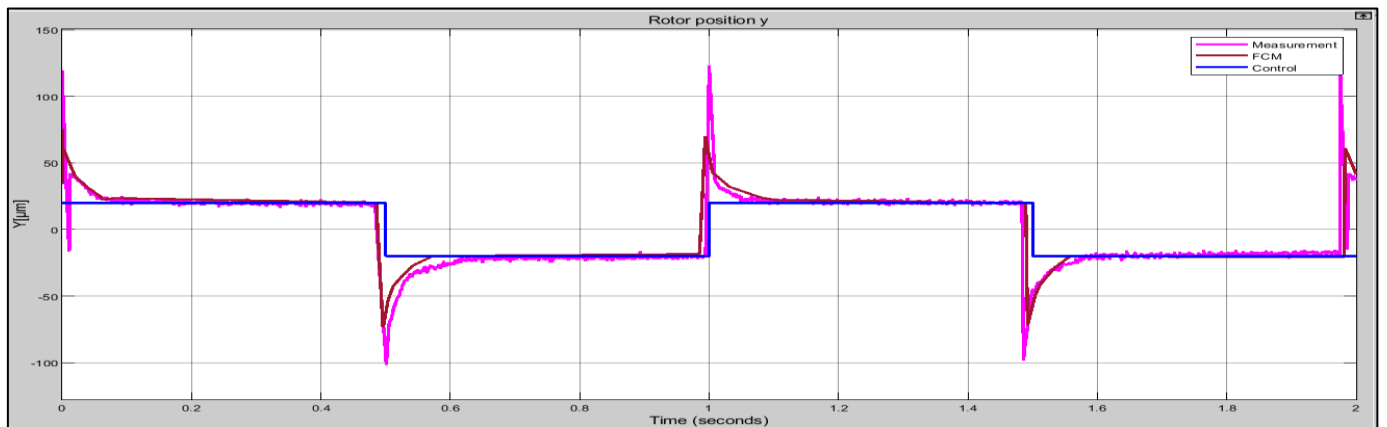

Fig 10 The Time Responses Results of the Control Currents: (d) Step Change is ±20µm of the Position of the Rotor

The precision of FCM is evaluated by computing the Root-Mean-Squared-Errors denoted by (RMSEs) between the measured values and simulations. Thus, they are computed using specific mathematical expressions as follows. Note that n represents the number of data points used in the measurements when calculating the Root Mean Squared Errors (RMSEs).

$$RMSE_x = \sqrt{\frac{1}{n}\sum_{k=1}^{n}[x_{measurement}(k) - x_{simulation}(k)]^2} \quad (20\,a)$$

$$RMSE_{ix} = \sqrt{\frac{1}{n}\sum_{k=1}^{n}[i_{x,measurement}(\ ) - i_{x,simulation}(k)]^2} \quad (20\,b)$$

$$RMSE_y = \sqrt{\frac{1}{n}\sum_{k=1}^{n}[y_{measurement}(k) - y_{simulation}(k)]^2} \quad (20\,c)$$

$$RMSE_{iy} = \sqrt{\frac{1}{n}\sum_{k=1}^{n}[i_{y,measurement}(k) - i_{y,simulation}(k)]^2} \quad (20\,d)$$

Table 3 lists the RMSEs values computed for the transient responses shown in Figures 9 and 10. It can be observed that the errors are smaller on the y-axis.

Table 3 RMSE Regarding Transient Responses

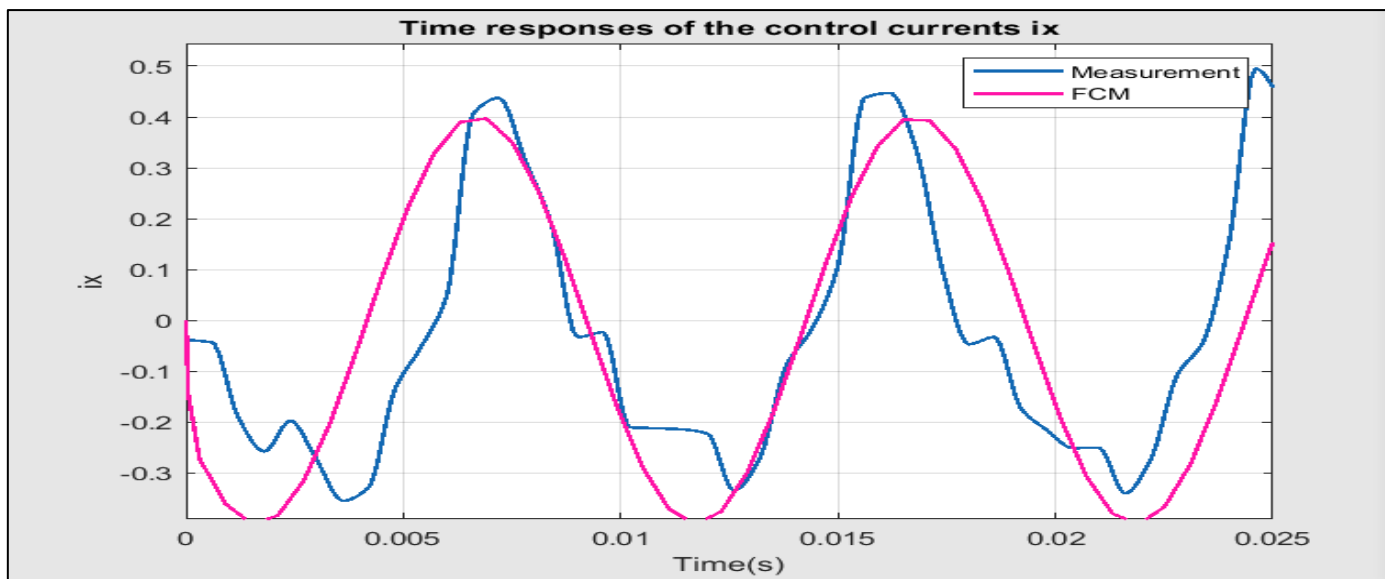|	$RMSE_x$	$RMSE_{ix}$	$RMSE_y$	$RMSE_{iy}$
A step change in the position of the rotor in the x-axis.	7.512 µm	111.2 mA	2.726 µm	50.72 mA
A step change in the position of the rotor in the y-axis.	2.378 µm	40.01 mA	4.081 µm	82.79 mA

Fig 11 The Variation of Control Currents (Ix) Over Time for Rotor Rotating at a Frequency Equal to 100 Hz.

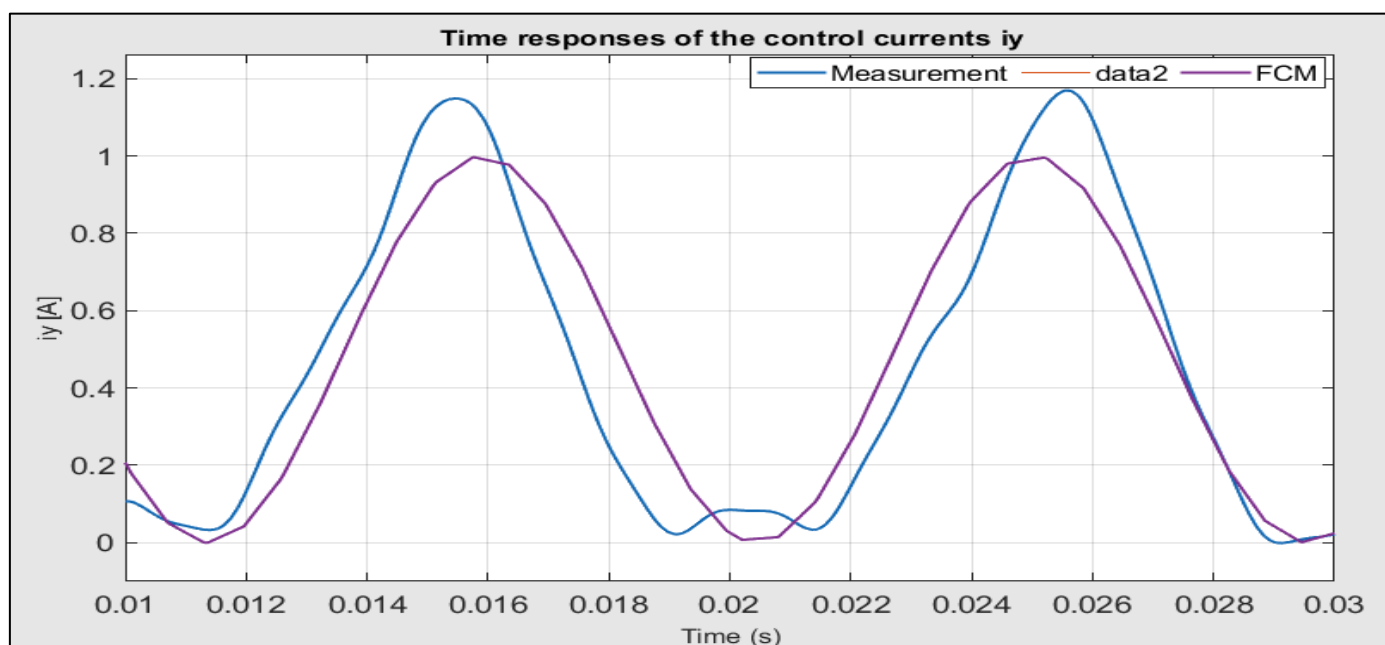Fig 12 The Variation of Control Currents (Iy) Over Time for Rotor Rotating at a Frequency Equal to 100 Hz.

Figures 11 and 12 show the control currents of the rotor when it is rotating at a 100 Hz frequency value, while Figure 13 shows the rotors' position in both axes for the same rotation. It is observed that the rotor motion's trajectory, as found based on the FCM and measurements, is not a perfect circle. The rotor movement's trajectory is not a perfect circle because of the asymmetrical magnetic force nature in the y-axis. Thus, both electrical and mechanical run-out lead to an unbalanced rotation of the oscillations and rotor in the control currents.
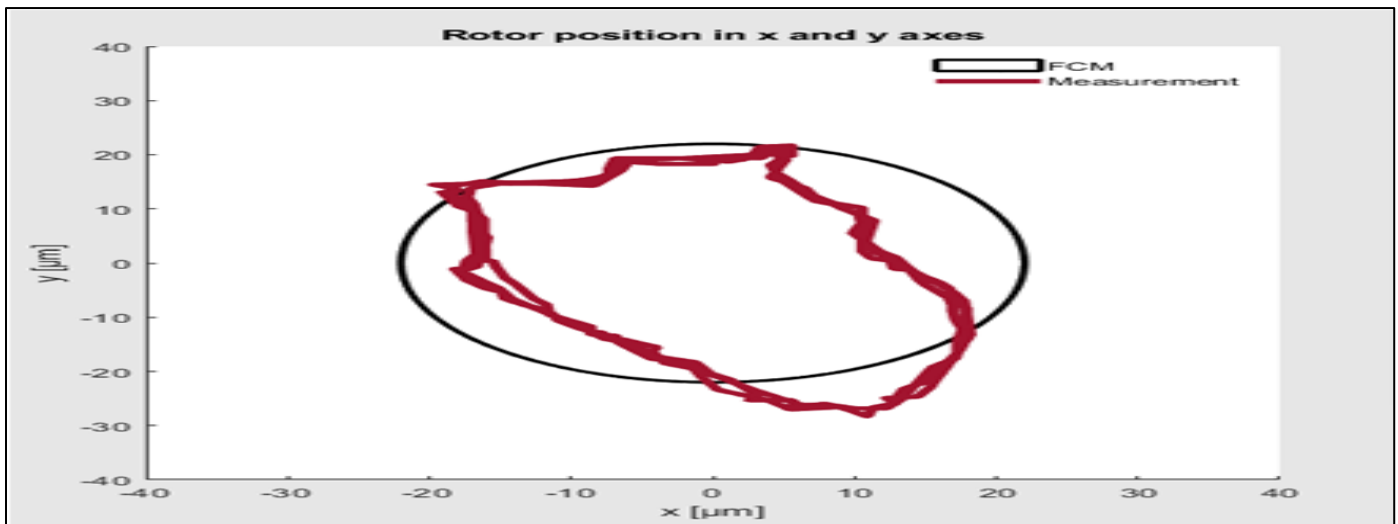
Fig 13 The Rotor Position in both Axes as it Rotates at a 100 Hz Frequency Value.

VII. CONCLUSION

In this study, modelling and analysis of a field-circuit model for the HMB were implemented to simulate the transient condition. This research employed an electromagnetic model of a 3D finite element with mechanics and electrical circuit equations. The model includes the complicated circuit magnetic of HMB shape and the nonlinear characteristic. The calculation of the magnetic field's outcomes is integrated to acquire the simulation model, which is utilised as a look-up table. After conducting the proposed method, several advantages exist, such as the short time to calculate the desired analysis and the low effort to compute the required performance. Therefore, these advantages return to the parameters of the proposed system that are computed once. The simulation model section involves desired controllers to levitate the magnetic bearing. In addition, the comparison between the rotor location and control currents assisted the verification of the simulated model. The real object is to test several control schemes and the proposed simulation model that achieved satisfactory results.

REFERENCES

[1.] Badics, Z. & Cendes, Z., 2007. Source field modelling by mesh incidence matrices. p. 1241–1244.
[2.] Han, B., 2014. Modeling and analysis of coupling performance of dynamic stiffness models for a novel combined radial-axial hybrid magnetic bearing. *Mathematical Problems in Engineering.*
[3.] Han, B. & Zheng, . S., 2013. Modeling and Analysis of Coupling Performance Between Passive Magnetic Bearing and Hybrid Magnetic Radial Bearing for Magnetically Suspended Flywheel.
[4.] Jabbar, M. A., Liu, Z. & Dong, J., 2003. Time-stepping finite-element analysis for the dynamic performance of a permanent magnet synchronous motor. *IEEE transactions on magnetics,* 39(5), pp. 2621-2623.
[5.] Jin, C., Su, H. & Dong, Y., 2022. Iron loss analysis of magnetic bearing system considering magnetic-thermal coupling. *International Journal of Applied Electromagnetics and Mechanics.*
[6.] Kushwah, M. & Patra, A., 2014. Tuning PID controller for speed control of DC motor using soft computing techniques-A review.. *Advance in Electronic and Electric Engineering,* 4(2), pp. 141-148.
[7.] Lomonova, E. A., 2010. Advanced actuation systems—State of the art: Fundamental and applied research. *In 2010 International Conference on Electrical Machines and Systems IEEE,* pp. 13-24.
[8.] Noshadi, A., 2019. Unbalance and Harmonic disturbance attenuation of a flexible shaft with active magnetic bearings. *Mechanical Systems and Signal Processing.*
[9.] Premkumar, K. et al., 2019. Fuzzy anti-windup pid controlled induction motor.. *International Journal of Engineering and Advanced Technology,* 9(1), pp. 184-189.
[10.] Samanta, P. & Hirani, H., 2022. On the evolution of passive magnetic bearings. Journal of Tribology. 144(4).
[11.] Shi, Q. & Dong, Y., 2022. Analysis of electromagnetic vibration and noise of permanent magnet synchronous motor based on field-circuit coupling. *Journal of Vibroengineering.*
[12.] Singh, S. & Tiwari, R., 2018. Model based identification of crack and bearing dynamic parameters in flexible rotor systems supported with an auxiliary active magnetic bearing. *Mechanism and Machine Theory,* Volume 122, pp. 292-307.
[13.] Srinivas, R. S., Tiwari, R. & Kannababu, C., 2018. Application of active magnetic bearings in flexible rotordynamic systems–A state-of-the-art review.. *Mechanical Systems and Signal Processing,* Volume 106, pp. 537-572.
[14.] Szelag, W., Jedryczka, C. & Myszkowski, A., 2023. Coupled Field Analysis of Phenomena in Hybrid Excited Magnetorheological Fluid Brake.

[15.] Tomczuk, B. & Koteras, D., 2015. 3D Field Analysis in 3-phase amorphous modular transformer. *Archives of Electrical Engineering, 64(1):119–127, 2015.,* p. 119–127.

[16.] Wajnert, D., 2019. A field-circuit model of the hybrid magnetic bearing. *Archive of Mechanical Engineering,* 66(2).

[17.] Wajnert, D., 2019. Comparison of two constructions of hybrid magnetic bearings. *Prz. Elektrotechniczn,* Volume 95, pp. 53-58.

[18.] Wajnert, D. & Tomczuk, B., 2019. Nonlinear magnetic equivalent circuit of the hybrid magnetic bearing . *COMPEL-The international journal for computation and mathematics in electrical and electronic engineering,* 38(4), pp. 1190-1203.

[19.] Zhou, R., Li, G., Wang, Q. & He, J., 2020. Torque calculation of permanent-magnet spherical motor based on permanent-magnet surface current and Lorentz force. *IEEE Transactions on Magnetics,* 56(5), pp. 1-9.

[20.] Zhu, Z. Q. et al., 2017. Analysis and reduction of unipolar leakage flux in series hybrid permanent-magnet variable flux memory machines. *IEEE Transactions on Magnetics,* 53(11), pp. 1-4.